# Nonlocal twist sequences in floppy kagome chains

Pegah Azizi and Stefano Gonella*
*Department of Civil, Environmental, and Geo- Engineering, University of Minnesota, Minneapolis, Minnesota 55455, USA*

(Received 17 May 2024; revised 19 July 2024; accepted 13 August 2024; published 3 September 2024)

The twisted kagome family comprises a spectrum of configurations that can be realized through the sweep of a single configurational degree of freedom known as a twist angle. Recently, it was shown that certain pairs of configurations along this sweep were linked by duality transformations and displayed matching phonon spectra. In this work, we introduce an intercell-connection system that spreads the lattice in the dimension orthogonal to the tessellation plane. The resulting three-dimensional character of the lattice allows us to sweep the entirety of the twist-angle spectrum, including all the compact configurations featuring overlapping triangles that, in a strictly two-dimensional space, are forbidden. Duality provides precious guidance for interpreting the availability of floppy mechanisms arising in the compact configurations through the one-to-one correspondence with their expanded counterparts. Our focus is on the compact configuration corresponding to a null twist angle, where the lattice degenerates to a chain. From the perspective of the chain, several of the local connections between neighboring lattice cells play the role of nonlocal long-range interactions between cells of the chain. We demonstrate experimentally some peculiar behavior that results from such nonlocality, including a selective activation of floppy sequences that is informed by the direction of loading.

DOI: 10.1103/PhysRevApplied.22.034001

## I. INTRODUCTION

Mechanical metamaterials are structural material systems deriving their properties and functionalities primarily from structural design rather than chemical composition [1–7]. Among them, lattice metamaterials may consist of periodic networks of springs and lumped masses, trusses of rods connected by ideal hinges or frames of beams [8–10]. Their stability depends on the coordination number, $z$, representing the average number of connections available at each node. Lattices are classified in $D$-dimensional space as under- ($z < 2D$), over- ($z > 2D$), and critically coordinated ($z = 2D$); the latter case is referred to as a Maxwell lattice [11,12]. Undercoordinated lattices accommodate deformation modes with zero elastic energy, termed *floppy modes*, wherein stresses are not stored in the bonds. On the other hand, overcoordinated systems lack floppy modes, aside from rigid-body motion [13,14]. Maxwell lattices feature the richest behavior, whereby they may support floppy modes, either in the bulk or on the edges, according to their specific cell geometry and boundary conditions [15–18].

Among two-dimensional (2D) Maxwell lattices, kagome lattices feature a unit cell comprised of two triangles connected at a vertex [19–23]. The kinematics of the kagome family is described by the relative twist angle, $\theta$. For instance, rotating two equilateral triangles by 180° yields the regular kagome lattice, which features three directions—relatively rotated by 60°—along which the bonds align perfectly, forming continuous load-carrying "fibers" that support states of self-stress (SSS). The SSS directions also support bulk floppy modes, which, to the leading-order approximation, involve alternating rotations of the bonds located along the fibers. These bulk floppy modes appear in the lattice band diagram as a flat zero-frequency branch for wave vectors along the $\Gamma - M$ direction of the irreducible Brillouin zone (BZ) contour [24]. In contrast, alternative angles result in twisted kagome configurations that lack SSS, lifting the phonon spectrum to finite frequencies for all wave vectors—except at the origin [25]. In practice, the twist-angle sweep corresponds to a global nonlinear soft mode, known as the Guest-Hutchinson mode, which deploys the lattice progressively from a compact to an expanded state [26–28].

Recently, Fruchart *et al.* discovered a special form of duality within the twisted kagome family, which could be ascribed to a hidden nonspatial symmetry [29]. This duality links pairs of distinct configurations that are equidistant in configuration space (along the sweep axis) from a critical $\theta_c$ value. Specifically, for a given configuration with twist angle $\theta$, there exists a dual with angle $\theta^*$, such that $\theta + \theta^* = 2\theta_c$, featuring an identical band diagram [29]. The critical configuration separating the dual sets, with $\theta_c = 90°$, maps to itself and is referred to as self-dual.

*Contact author: sgonella@umn.edu

 

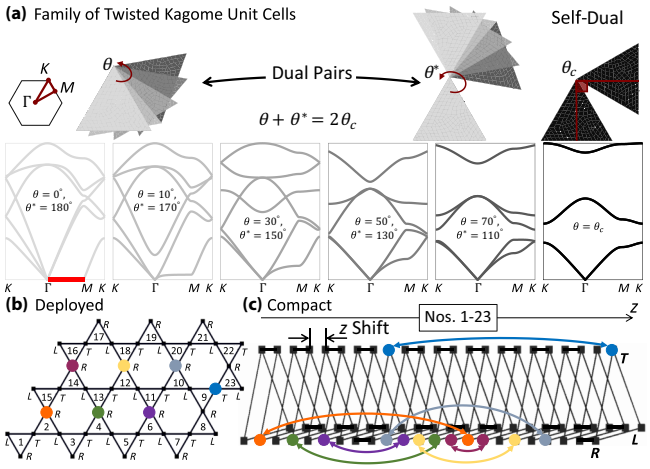


FIG. 1. (a) Sweep of twist angles highlighting dual pairs ($\theta$ and $\theta^*$) featuring identical band diagrams (color coded). Bulk floppy mode for the dual set ($\theta = 0^\circ, 180^\circ$) is highlighted in red. Self-dual configuration ($\theta_c = 90^\circ$) is reported on the right. Schematic representations of a finite kagome domain comprising 23 triangles shown in the deployed state for $\theta = 180^\circ$ (b) and in the compact state collapsing to a twist chain for $\theta = 0^\circ$ (c). Vertices are denoted as $T$, $L$, and $R$, and hinges connecting the rows of cells are color coded to illustrate their migration along the chain axis.

Despite sharing the same space-group symmetry with other pairs, the self-dual configuration showcases unique properties, such as double degeneracy for all phonons across the entire BZ [29–31]. Duality is observed in ideal lattices, such as spring-mass or trusslike lattices [31–33]. The phenomenon is summarized in Fig. 1(a) for the case of solid elastic triangles connected by perfect hinges, where the triangles can deform internally according to 2D plane-stress elasticity, while maintaining the ability to rotate freely, thus enjoying the hinge-ideality conditions required by duality. Indeed, we can see that dual pairs exhibit overlapping spectra.

The motivation for this study stems from an attempt to explore holistically the *entire* twisted kagome family, delving into potentially unconventional phenomena that emerge from its collapse into compact states, interpreting the mechanics of any emergent configurations through the lens of duality. Recall that, as we sweep the twist angle, the lattice transitions from a deployed state ($\theta = 180^\circ$) to a compact state ($\theta = 0^\circ$). Our investigation focuses on this extreme dual pair. Notably, duality ensures that both the $180^\circ$ and $0^\circ$ configurations feature floppy bulk modes along the high-symmetry line, $\Gamma$-$M$ (see S1 within the Supplemental Material [34]). While the manifestation of such modes in the deployed lattice is well understood, one may ask how the phenomenon manifests in the compact case, and whether, in such a case, the kinematics of the bulk floppy mode can give rise to new structural logic functionalities.

## II. COLLAPSING 2D KAGOME LATTICES INTO 1D KAGOME CHAINS

To address this question, we propose a variation of the conventional twisted kagome specifically designed to elucidate the mechanics of the compact configuration. This task immediately involves a practical challenge: while, in principle, all values of $\theta$ are allowed, practical constraints require that $\theta$ does not exceed values at which two triangles come into contact, i.e., the $\theta < 60^\circ$ and $\theta > 300^\circ$ ranges are forbidden. This restriction becomes more severe in structural lattices [30,35,36], where the finite thickness of the beamlike bonds and filleted joints at the internal clamps prevent tight reentrant angles, even in the permissible $\theta$ range. To circumvent this limitation, we propose a modified kagome arrangement in which we let pairs of triangles that exchange forces at a shared hinge be shifted by a finite amount, $d$, in the out-of-plane $z$ direction. This modification enables them to rotate *freely* on *parallel* $z$-shifted planes. The *coplanar* mechanics of the system follow the same elasticity rules of the in-plane mechanics of the original kagome lattice, albeit featuring an additional dependence on the $z$ coordinate. For the sake of illustration, let us assume the deployed state of a finite domain consisting of $n \times m$ unit cells, numbered according to a semi-row-wise pattern, as shown in Fig. 1(b) for $n = 3$ and $m = 4$. Removing the last dangling triangle, we have a total of $2nm - 1 = 23$ triangles. Subsequently, we systematically apply the $z$ shift monotonically at the contact hinge of every consecutive pair along the assumed sequence, resulting in a total depth of $2d(nm - 1)$. Note that, if we reconfigure the lattice towards the compact state by applying a global soft mode, the signs of the twist angles alternate along the sequence, which therefore can be seen as the lattice *deployment sequence*.

In the compact case at $\theta = 0^\circ$, all triangles collapse and align to form a one-dimensional (1D) prismatic structure with a layout and kinematics akin to those of a chain capable of deforming through the relative rotation of its triangular cross sections, as shown in Fig. 1(c). Unlike conventional torsional chains, rotations here do not occur about a shared axis, but rather about three distinct parallel axes passing through the hinges labeled $T$, $L$, and $R$ in Figs. 1(b) and 1(c), at the top, left, and right corners, respectively. One of the most striking consequences of collapsing the kagome into a chain is the emergence of *nonlocal* interactions. According to the deployment sequence, in-plane triangles that are mechanically connected and belong to the same row of the deployed lattice occupy adjacent positions in the chain, establishing local interactions along its axis. In contrast, those belonging to different rows are positioned farther apart in the chain, resulting in nonlocal interactions. Alternatively, the numbering strategy dictates that some connections between adjacent pairs of triangles in the planar case involve consecutive indices

and incremental $z$ coordinates in the chain, while others feature discrete jumps, marked by finite gaps in $z$. Specifically, seven nonlocal connections are identified and color coded in Figs. 1(b) and 1(c). It is important to note that the physical nature of the connection does not change between Figs. 1(b) and 1(c). Nevertheless, nonlocality endows selected connections with a new functionality when we interpret their kinematics from the perspective of the twist mechanics of the chain. In other words, without introducing any change in the kinematics, nearest neighbors in the 2D lattice become non-nearest neighbors along the axis of the chain (see S2 within the Supplemental Material [34]).

Duality guarantees that the phonon spectrum of the coplanar dynamics of the chain ($\theta = 0°$) matches that of the in-plane dynamics of its dual counterpart ($\theta = 180°$) and should therefore also exhibit bulk floppy modes. Notably, within the finite domain in Fig. 1(b), we identify 13 straight lines aligned along the *T*-*R*, *L*-*R*, and *L*-*T* directions, associated with the Γ-*M* direction, that support bulk floppy modes. To understand how these modes manifest within the 23-cell chain, we conduct static simulations, constraining one edge of the first and last triangles and loading a randomly selected triangle (No. 12) with a unit-amplitude force. We conduct three sets of simulations, loading the *T* point along the *T*-*R* direction, the *L* point along *L*-*R*, and the *L* point along *L*-*T*. The resulting twist sequences are shown in Figs. 2(a)–2(c). We observe that, in each case, the twist sequence involves triangles corresponding to those clustered along the selected direction of aligned bonds passing through triangle No. 12 in the deployed state. For instance, loading the *T* point along *T*-*R* [Fig. 2(a)] mainly induces the twist of the (3-4-12-13-18-19) sequence. Similarly, loading along *L*-*R* [Fig. 2(b)] activates the (6-7-11-12-17-18) sequence (see S3 within the Supplemental Material [34] for the deployed state). Interestingly, as a result of nonlocality, the activation sequence involves some sets of nonconsecutive triangles. In contrast, loading along *L*-*T* results in a predominantly compact twist sequence, as the *L*-*T* triangles are linked by local connections in the chain. We repeat this exercise for triangle No. 16, observing similar behavior, see Figs. 2(d) and 2(e).

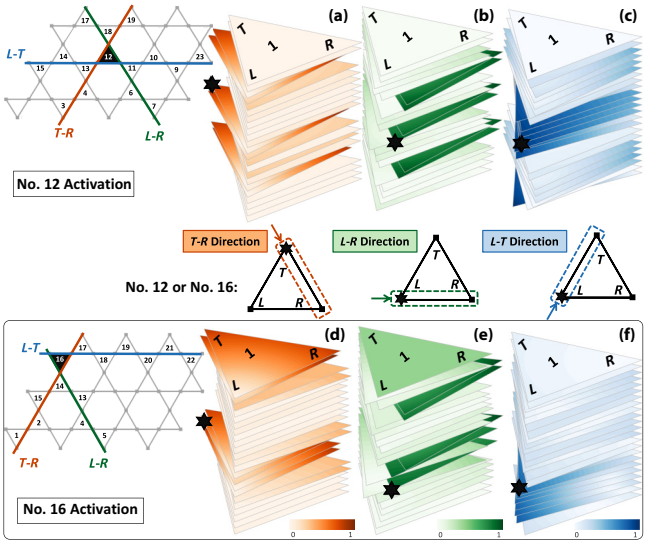


FIG. 2. Full-scale static simulation results for 23-cell chains (and corresponding deployed lattices) loaded at triangles No. 12 and No. 16 along the (a),(d) *T*-*R*; (b),(e) *L*-*R*; and (c),(f) *L*-*T* directions. Triangles are colored according to the magnitude (normalized by highest) of their twist. Activated triangles match the selected directions in the deployed lattices.

## III. EXPERIMENTS ON THE KAGOME-CHAIN PROTOTYPE

Seeking experimental verification of the result in Fig. 2 requires overcoming the nontrivial fabrication challenge of realizing a physical prototype endowed with all the nonlocal interactions required by the model. After several iterations, our design process lands on the prototype illustrated in Fig. 3(a), which is shown along with schematics of the hinge components. The triangles are water-jet cut from an aluminum slab and connected to their neighbors via pin hinges. Each hinge comprises a shaft connected through washers and screws to roller bearings that guarantee virtually frictionless rotations and minimize any jiggling that would cause loss of coaxiality. The nonlocal interactions are realized through arm links that stem from the hinges they are intended to connect; these are free to rotate with respect to them but rigidly attached to long bars that are properly offset from the chain. The flat sections are tightly fastened at each end of the bar using small screws and thread lockers to prevent loosening over loading cycles. This setup allows coaxiality to be maintained between the vertices that should remain connected at all stages of deployment, without interfering with those that are only aligned at $\theta = 0°$. Two snapshots capturing different views of the deployment of the chain are provided in the inset of Fig. 3(a) (details are given in S4 within the Supplemental Material [34]).

To subject the prototype to mechanical testing, we need to circumvent a practical challenge. As fabricated, the chain is unstable, tending to automatically deploy to its expanded state if left unconstrained. This issue arises from the interplay between gravity and the geometric eccentricity of the specimen, due to the nonlocal connections, which concur to exert a torque on the chain that is not resisted by the nearly frictionless hinges. The problem is especially pronounced if the chain is hung vertically. To curb the issue, we propose a setup where the chain rests horizontally on a flat surface. Figures 3(b)–3(g) illustrate the behavior of the chain when loaded statically at triangles No. 12 [Figs. 3(b)–3(d)] and No. 16 [Figs. 3(e)–3(g)]. The load is applied manually by pulling the desired corner (*T* or *L*) of the specified triangle (No. 12 or No. 16) along the intended

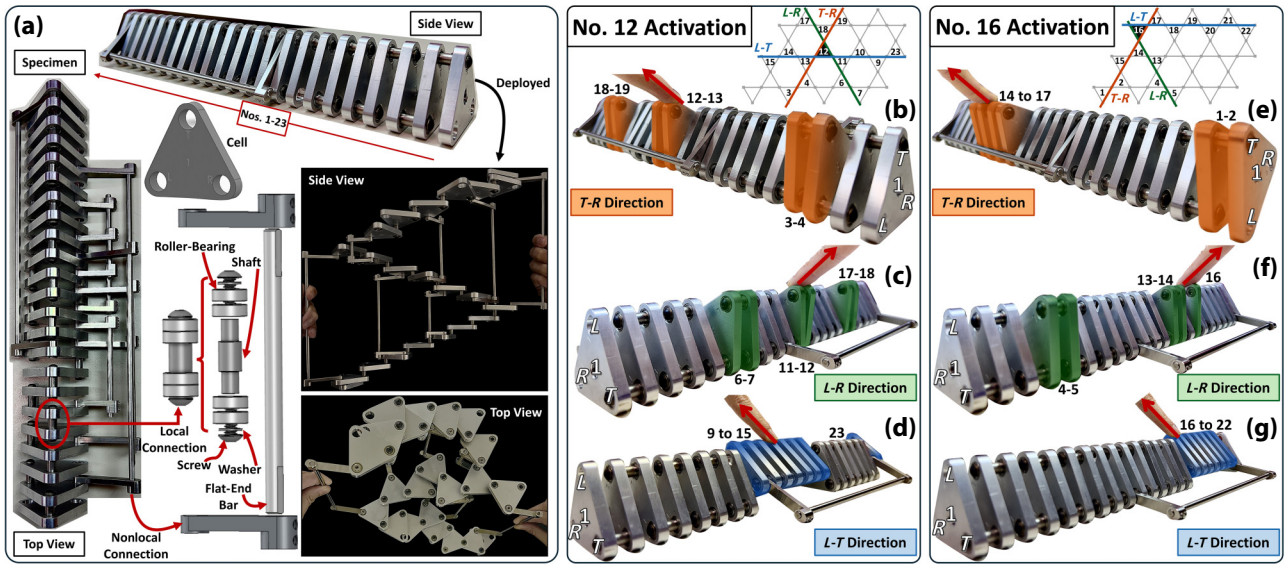


FIG. 3. (a) Top and angled views of the chain prototype, along with magnified details of its components, highlight the technology involved in realizing nonlocal long-range intercell connections. Insets show side and top views of the prototype during deployment. Snapshots from static experiments with loading applied at triangles No. 12 (b, c, d) and No. 16 (e, f, g), along the (b),(e) *T*-*R*; (c),(f) *L*-*R*; and (d),(g) *L*-*T* directions. Results show activation sequences of triangles corresponding to the three floppy-mode directions of the deployed state. System allows switching between local activation (d),(g) and nonlocal activation (b),(c),(e),(f) through a simple flip of the loading direction.

direction (*T*-*R*, *L*-*R*, or *L*-*T*). Note that we orient the entire specimen according to the corner intended for loading. For instance, to load the *T* corner [Figs. 3(b) and 3(e)], the specimen is aligned such that the *L*-*R* side rests on the surface. Conversely, to load the *L* corner [Figs. 3(c), 3(d), 3(f), and 3(g)], the *T*-*R* side is laid on the surface.

Throughout the loading process, we ensure that the specimen is not lifted from the surface nor slides on it. This is achieved by ensuring the vertical component ($F_Y$) of the load (**F**) does not exceed the weight of the chain (**W**) and maintains the horizontal reaction force (**T**), which balances the horizontal component of the load ($F_X$), below the maximum allowable force without sliding ($\mathbf{T} < \mathbf{T}_{\max} = \mu_s \mathbf{N}$, where **N** is the vertical reaction from the surface and $\mu_s$ is the coefficient of static friction). These conditions, graphically depicted in Fig. 4(a), are easily met by working with a sufficiently frictional surface and a heavy chain (as in our study). Under these equilibrium conditions, the load boils down to a moment about one of the vertices resting on the surface, which, in the absence of sliding, can be treated as a pin support (details of SolidWorks animations are given in S5 within the Supplemental Material [34]). Accounting for the kinematics of the setup requires a revision of the boundary conditions with respect to those assumed in the simulations of Fig. 2 (see S6 within the Supplemental Material [34]). This adjustment can be enforced by pinning all the triangle corners of the lattice that, in the deployed state, do not lie along lattice directions parallel to the applied load. For example, all *L* corners should be pinned when we load along the *T*-*R* direction. A simulation of the deployed state, incorporating the revised boundary conditions, is shown in Fig. 4(b) for *T*-*R* loading, showing the manifestation of soft modes under the additional constraints. For simulations for other loading cases, see S7 within the Supplemental Material [34].

With the kinematics of the horizontal chain figured out, we can interpret the results shown in Figs. 3(b)–3(d) for triangle No. 12. We observe that the behavior agrees with the predictions from the band diagram and static simulation. For each direction of loading, only the triangles that are located along the loading direction in the deployed state are activated along the chain. This effect has an unexpected consequence. Since the modes directed along the

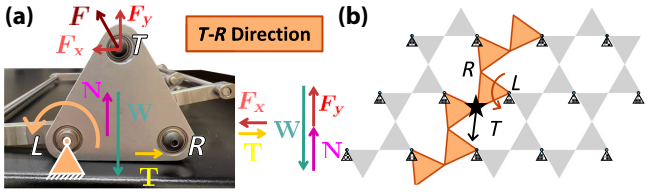


FIG. 4. (a) Graphical illustration of the static equilibrium considerations involved in modeling the interaction of the chain with its underlying support. Free-body diagram depicts the forces on the prototype when loading the *T* corner along *T*-*R*. (b) Static simulation of the corresponding deployed lattice for *T*-*R* loading, incorporating updated boundary conditions inspired by the kinematics illustrated in (a).

three floppy directions involve different sets of triangles, which are differently distributed along the length of the chain, the selection of a direction of loading results in the activation of qualitatively different twist sequences. Those along *T*-*R* and *L*-*R* involve distributed nonlocal twist patterns, while the one along *L*-*T* results, by and large, in a localized clustered pattern. In essence, the chain displays an ability to switch between local and nonlocal activation sequences that are controlled solely by the selected direction of loading. Similar considerations can be made for triangle No. 16 in Figs. 3(e)–3(g).

## IV. DISCUSSION ON LOAD-DIRECTION SELECTIVITY

To emphasize the ability of the system to switch between local and nonlocal effects based solely on the direction of loading, let us revisit the problem using longer chains associated with larger lattice domains. We simulate chains with increasing cell numbers (30, 54, 78, 102), as shown in Fig. 5. We start with a 30-cell chain, corresponding to a $3 \times 5$ deployed configuration. For each subsequent scenario, we add four columns to the previous deployed configuration, and we determine the necessary hinge connectivity for the corresponding chain. We then subject the center triangle of each chain to a unit-amplitude force applied at the *T* corner, targeting the *T*-*R* and *L*-*T* loading directions. The resulting twist patterns for *T*-*R* and *L*-*T* are depicted in Figs. 5(a) and 5(b), respectively. Observation of the results allows us to formulate a simple rule governing the relationship between the activation sequence and the lattice dimensionality and layout. For a finite *n*-row by *m*-column domain, *T*-*R* or *L*-*R* loading yields a distributed response featuring *n* peaks, each encompassing two triangles, while *L*-*T* loading activates a localized response involving a cluster of $2m$ triangles.

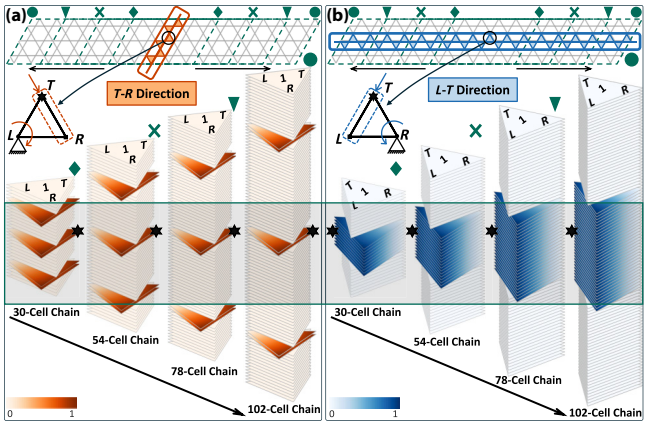


FIG. 5. Parametric study revealing exacerbation of the dichotomy between local (b) and nonlocal twist sequences (a) in chains of increasing cell numbers. Deployed configurations of the different chains depicted at the top of each panel show that longer chains correspond to finite lattices with more columns and equal numbers of rows. Shaded box outlines a 31-cell interval around the load. As the chain lengthens, nonlocal activation sequences (a) shift progressively away from the load, while local ones (b) retain clustering.

We noted above that varying the loading direction could lead to an abrupt switch between localized and distributed activation sequences. As the chain length increases, nonlocal activations due to *T*-*R* loading propagate further from the loaded cell. This is quantified by considering a control window encompassing approximately 31 cells, centered around the loaded cell, as shown in Fig. 5. In contrast, for *L*-*T* loading, the twisted cluster remains localized and tends to occupy a progressively larger portion of the control window. In other words, the dichotomy between local and nonlocal effects grows. At the limit of an infinite lattice, when we load along *T*-*R*, all the nonlocal activations shift indefinitely outwards, away from the loading spot, and the response reduces to the twist of the loaded triangle and the adjacent one. When we load along *L*-*T*, the cluster of twisted triangles grows indefinitely, encompassing an increasingly long portion of the chain about the loading point. In summary, we establish a total dichotomy between an extremely localized response for *T*-*R* loading and a distributed response for *L*-*T* loading. Such dichotomy can only be appreciated through the lens of the chain dynamics, where the interaction landscape embedded in the lattice cell sequence manifests in the form of nonlocality.

## V. CONCLUSION

In this work, we documented the emergence of a series of unintuitive activations of floppy mechanisms, resulting from emerging nonlocality in kagome chains obtained by collapsing regular kagome lattices into their fully compact states via the Guest-Hutchinson mode. Nonlocality produces marked dichotomies in the chain mechanisms that are sensitive to the direction of loading, yielding an unprecedented selective character of the chain torsional response.

## ACKNOWLEDGMENTS

The authors acknowledge support from the National Science Foundation (Grant No. CMMI-2027000). The authors are grateful to K. Sun and S. Sarkar (University of Michigan) for insightful discussions and to Peter Ness and Max Olson (University of Minnesota CSE Shop) for precious assistance with prototype design and fabrication.

[1] Jae-Hwang Lee, Jonathan P. Singer, and Edwin L. Thomas, Micro-/nanostructured mechanical metamaterials, Adv. Mater. **24**, 4782 (2012).

[2] Sahab Babaee, Jongmin Shim, James C. Weaver, Elizabeth R. Chen, Nikita Patel, and Katia Bertoldi, 3D soft metamaterials with negative Poisson's ratio, Adv. Mater. **25**, 5044 (2013).

[3] Johan Christensen, Muamer Kadic, Martin Wegener, Oliver Kraft, and Martin Wegener, Vibrant times for mechanical metamaterials, MRS Commun. **5**, 453 (2015).

[4] A. Rafsanjani and D. Pasini, Bistable auxetic mechanical metamaterials inspired by ancient geometric motifs, Extreme Mech. Lett. **9**, 291 (2016).

[5] Katia Bertoldi, Vincenzo Vitelli, Johan Christensen, and Martin van Hecke, Flexible mechanical metamaterials, Nat. Rev. Mater. **2**, 17066 (2017).

[6] B. Deng, J. R. Raney, V. Tournat, and K. Bertoldi, Elastic vector solitons in soft architected materials, Phys. Rev. Lett. **118**, 204102 (2017).

[7] Bolei Deng, Siqin Yu, Antonio E. Forte, Vincent Tournat, and Katia Bertoldi, Characterization, stability, and application of domain walls in flexible mechanical metamaterials, Proc. Natl. Acad. Sci. **117**, 31002 (2020).

[8] L. Brillouin, *Wave Propagation in Periodic Structures: Electric Filters and Crystal Lattices*, 2nd revised ed. (Dover Publications, New York, 1953), https://archive.org/details/wavepropagationi0000bril.

[9] A. Srikantha Phani, J. Woodhouse, and N. A. Fleck, Wave propagation in two-dimensional periodic lattices, J. Acoust. Soc. Am. **119**, 1995 (2006).

[10] Michael Czajkowski, Corentin Coulais, Martin van Hecke, and D. Zeb Rocklin, Conformal elasticity of mechanism-based metamaterials, Nat. Commun. **13**, 211 (2022).

[11] J. Clerk Maxwell, On the calculation of the equilibrium and stiffness of frames, London, Edinburgh, Dublin Philos. Mag. J. Sci. **27**, 294 (1864).

[12] C. R. Calladine, Buckminster Fuller's "tensegrity" structures and Clerk Maxwell's rules for the construction of stiff frames, Int. J. Solids Struct. **14**, 161 (1978).

[13] M. F. Thorpe, Continuous deformations in random networks, J. Non. Cryst. Solids **57**, 355 (1983).

[14] Robert Connelly, Generic global rigidity, Discrete Comput. Geom. **33**, 549 (2005).

[15] T. C. Lubensky, C. L. Kane, Xiaoming Mao, A. Souslov, and Kai Sun, Phonons and elasticity in critically coordinated lattices, Rep. Prog. Phys. **78**, 073901 (2015).

[16] Xiaoming Mao and T. C. Lubensky, Coherent potential approximation of random nearly isostatic kagome lattice, Phys. Rev. E **83**, 011111 (2011).

[17] C. L. Kane and T. C. Lubensky, Topological boundary modes in isostatic lattices, Nat. Phys. **10**, 39 (2014).

[18] Xiaoming Mao and Tom C. Lubensky, Maxwell lattices and topological mechanics, Ann. Rev. Condens. Matter Phys. **9**, 413 (2018).

[19] Marshall Schaeffer and Massimo Ruzzene, Wave propagation in reconfigurable magneto-elastic kagome lattice structures, J. Appl. Phys. **117**, 194903 (2015).

[20] Katia Bertoldi, Vincenzo Vitelli, Johan Christensen, and Martin van Hecke, Flexible mechanical metamaterials, Nat. Rev. Mater. **2**, 17066 (2017).

[21] H. Chen, H. Nassar, A. N. Norris, G. K. Hu, and G. L. Huang, Elastic quantum spin Hall effect in kagome lattices, Phys. Rev. B **98**, 094302 (2018).

[22] E. Riva, D. E. Quadrelli, G. Cazzulani, and F. Braghin, Tunable in-plane topologically protected edge waves in continuum kagome lattices, J. Appl. Phys. **124**, 164903 (2018).

[23] Hussein Nassar, Hui Chen, and Guoliang Huang, Microtwist elasticity: A continuum approach to zero modes and topological polarization in kagome lattices, J. Mech. Phys. Solids **144**, 104107 (2020).

[24] Anton Souslov, Andrea J. Liu, and T. C. Lubensky, Elasticity and response in nearly isostatic periodic lattices, Phys. Rev. Lett. **103**, 205503 (2009).

[25] Kai Sun, Anton Souslov, Xiaoming Mao, and T. C. Lubensky, Surface phonons, elastic response, and conformal invariance in twisted kagome lattices, Proc. Natl. Acad. Sci. **109**, 12369 (2012).

[26] S. D. Guest and J. W. Hutchinson, On the determinacy of repetitive structures, J. Mech. Phys. Solids **51**, 383 (2003).

[27] D. Zeb Rocklin, Shangnan Zhou, Kai Sun, and Xiaoming Mao, Transformable topological mechanical metamaterials, Nat. Commun. **8**, 14201 (2017).

[28] Xuenan Li and Robert V. Kohn, Some results on the Guest–Hutchinson modes and periodic mechanisms of the kagome lattice metamaterial, J. Mech. Phys. Solids **178**, 105311 (2023).

[29] Michel Fruchart, Yujie Zhou, and Vincenzo Vitelli, Dualities and non-Abelian mechanics, Nature **577**, 636 (2020).

[30] Pegah Azizi, Siddhartha Sarkar, Kai Sun, and Stefano Gonella, Dynamics of self-dual kagome metamaterials and the emergence of fragile topology, Phys. Rev. Lett. **130**, 156101 (2023).

[31] Stefano Gonella, Symmetry of the phononic landscape of twisted kagome lattices across the duality boundary, Phys. Rev. B **102**, 140301 (2020).

[32] Qun-Li Lei, Feng Tang, Ji-Dong Hu, Yu-qiang Ma, and Ran Ni, Duality, hidden symmetry, and dynamic isomerism in 2D hinge structures, Phys. Rev. Lett. **129**, 125501 (2022).

[33] Michel Fruchart, Claudia Yao, and Vincenzo Vitelli, Systematic generation of Hamiltonian families with dualities, Phys. Rev. Res. **5**, 023099 (2023).

[34] See the Supplemental Material at http://link.aps.org/supplemental/10.1103/PhysRevApplied.22.034001 for additional details, including the band diagram, physical realization of the model, floppy-mode visualization, videos and details of the deployment process, SolidWorks animations, and static simulation of the compact and deployed states.

[35] Zi-Dong Zhang, Ming-Hui Lu, and Yan-Feng Chen, Twist-angle-induced boundary-obstructed topological insulator on elastic kagome metamaterials, Phys. Rev. Appl. **20**, 054002 (2023).

[36] P. Azizi, S. Sarkar, K. Sun, and S. Gonella, Omnidirectional domain wall modes protected by fragile topological states, Phys. Rev. B **110**, L060102 (2024).